

## Supporting Information

### Dynamic control of the location of nanoparticles in the hybrid co-assemblies

Zhilong Su<sup>[a]</sup>, Xiaokang Li<sup>[b]</sup>, Xuesong Jiang<sup>\*[a]</sup>, Shaoliang Lin<sup>\*[b]</sup>, Jie Yin<sup>[a]</sup>

a. School of Chemistry & Chemical Engineering, State Key Laboratory for Metal Matrix Composite Materials, Shanghai Jiao Tong University  
Shanghai 200240, China.

b. School of Materials Science and Engineering, East China University of Science and Technology, Shanghai 200237, China

Tel.: +86-21-54743268; Fax: +86-21-54747445. E-mail: [ponygle@sjtu.edu.cn](mailto:ponygle@sjtu.edu.cn);

[slin@ecust.edu.cn](mailto:slin@ecust.edu.cn)

#### 1. Experiments and Instruments

#### 2. DPD simulation method

#### 3. Results

#### 3.1 DSC thermograms of AN-hPEA, AN-POSS and their corresponding composites

#### 3.2 Cross-section TEM images, SEM images and DLS of CSM along thermal annealing at 85 °C for different times

#### 3.3 Corresponding spatial distribution of AN-POSS in CSM along the radius direction at different annealing timesteps according to DPD simulation.

#### 3.4 Fick's second law of diffusion to stimulate the diffusion of AN-POSS in CSM

#### 3.5 Photo-crosslinking of CSM through the photo-dimerization of AN

#### 3.6 Young's modulus of CSM determined by AFM

#### 4 References

#### 1. Experiments and Instruments

### **Preparation of core-shell hybrid microsphere and thermal annealing**

The preparation of core-shell microspheres was discussed in detail in our previous work.<sup>1</sup> Typically, 6.6 mg of AN-hPEA and 3.3 mg of AN-POSS were first dissolved into 1 mL of dioxane, which is a good solvent for both AN-hPEA and AN-POSS. The solution equilibrated at 25 °C for 1 hour before 9 mL of mili-Q water was added slowly to the solution (5 mL of water per hour). The polymer solution was gently stirred during the water addition process. Then, the samples were dialyzed against water for 24 h and collected for further treatment. The CSM described in this paper is not cross-linked unless specifically noted. In a typical annealing process, 10 ml of CSM aqueous solution (1 mg/ml) was filled in a 25 ml bottle. Then the CSM aqueous solution was placed in a precisely controlled heater (IKA RET Basic equipped with ETS-D5, Germany) under a gentle stir.

### **Scanning Electron Microscopy (SEM)**

The SEM images of assemblies were obtained using a Nova NanoSEM 450 (FEI Ltd., USA) field emission scanning electron microscope operated at an acceleration voltage of 5 kV. The samples were prepared by dropping the CSMs solution onto silica wafers, and dried at 25 °C for 48 h. Then the samples were sputter coated with Pt to minimize charging.

### **Transparent Electron Microscopy (TEM)**

The TEM images of co-assemblies were obtained using a JEM-2100 (JEOL Ltd., Japan) transmission electron microscope operated at an acceleration voltage of 200 kV. The sample was prepared by dropping the solution of co-assemblies onto copper grids (Carbon Film Only, 200 mesh, Xinxing Braim, china), and then dried at 25 °C for 48 h. No staining treatment was performed for the measurement. The Ultrathin sectioning of CSM for TEM analysis was carried out on Leica Ultracut UCT6 low temperature sectioning system (LEICA Co., GERMANY). The sectioning temperature is -120 °C.

### **Dynamic light scattering (DLS)**

DLS measurements were performed on the CSMs aqueous solutions using a ZS90 Zetasizer Nano ZS instrument (Malvern Instruments Ltd., U.K.) equipped with

a multi-s digital time correlation and a 4 mW He-Ne laser ( $\lambda=633$  nm) at an angle of  $90^\circ$ . The concentration of the CSMs for DLS analysis is 0.1 mg/mL.

### **Differential scanning calorimetry (DSC)**

All DSC thermograms of assemblies was carried out on a Q2000 Modulated Differential Scanning Calorimeter (TA, USA), the samples were run under flowing  $N_2$  and at a heating rate of  $10^\circ C/min$ . The samples were prepared by freeze drying of the solution of CSM.

### **Atomic Force Microscope (AFM)**

The AFM Imaging and Force Spectroscopy of assemblies were obtained using a Nanonavi E-Sweep (SII, Japan) with a scanning tube of  $150\ \mu m$  and a z range of  $4\ \mu m$ . AFM cantilevers ( $\mu masch$ ) made of silicon nitride with a spring constant of  $0.56\ N/m$  were used, half angle of the AFM tip is  $30^\circ$ . AFM imaging and force-curve measurements were performed in the drymode with wafer as a control. The surface morphologies of samples and force curves were acquired in the contact mode. The samples were prepared by dropping the solution of co-assemblies onto mica sheet, and dried at  $25^\circ C$  for 48 h.

The Data from the Force Curve Measurements was analyzed via the Hertz model relating to the indentation  $\delta$  with the loading force (F) <sup>2,3</sup>.

$$F = \frac{2}{\pi} \cdot E^* \cdot \delta^2 \cdot \tan\alpha$$

$$\frac{1}{E^*} = \frac{1 - \nu_1^2}{E_1} + \frac{1 - \nu_2^2}{E_2}$$

where  $E$  and  $\nu$  are the Young's modulus and Poisson ration, subscript 1 stands for sample while 2 for cantilever. The Poisson ration is assumed to be 0.5 for incompressible materials.  $\alpha$  is the half angle of the AFM tip. Since the diameter of the CSM in this study is over  $800\ nm$ , the fitting analysis range is  $z = 0 - 60\ nm$  (i.e., less than 10 % of the CSM height) of the force curves to determine  $E$  values.

To enhance the stability, the annealed CSM is cross-linked by irradiation of  $365\ nm$  UV-light before AFM measurement.

## 2. DPD simulation method

### Simulation Method

Dissipative particle dynamics is first proposed by Hoogerbrugge and Koelman,<sup>2,3</sup> which is suitable for complex fluids.<sup>4-7</sup> It is a combination of molecular dynamics, lattice-gas automata, and Langevin dynamics, which obeys Galilean invariance, isotropy, mass conservation, and momentum conservation. In the method, a bead having mass  $m$  represents a block or cluster of atoms or molecules moving together in a coherent fashion. The DPD beads are subject to soft potentials and governed by predefined collision rules.

In the method, the force  $\mathbf{f}_i$  acting on bead  $i$  is a pairwise additive force, consisting of the conservative force ( $\mathbf{F}_{ij}^C$ ), dissipative force ( $\mathbf{F}_{ij}^D$ ), and random force ( $\mathbf{F}_{ij}^R$ ), given by<sup>5</sup>

$$\mathbf{f}_i = \sum_{j \neq i} (\mathbf{F}_{ij}^C + \mathbf{F}_{ij}^D + \mathbf{F}_{ij}^R) \quad (1)$$

The conservative force is a soft repulsion taking the form as follows:

$$\mathbf{F}_{ij}^C = a_{ij} \sqrt{\omega(r_{ij})} \hat{\mathbf{r}}_{ij} \quad (2)$$

where  $a_{ij}$  is the maximum repulsive interaction between beads  $i$  and  $j$ ,  $\mathbf{r}_{ij} = \mathbf{r}_i - \mathbf{r}_j$ ,

$r_{ij} = |\mathbf{r}_{ij}|$ ,  $\hat{\mathbf{r}}_{ij} = \mathbf{r}_{ij}/r_{ij}$ , and  $\omega(r_{ij})$  is the weight function given by

$$\omega(r_{ij}) = \begin{cases} (1 - r_{ij}/r_c)^2 & (r_{ij} < r_c) \\ 0 & (r_{ij} \geq r_c) \end{cases} \quad (3)$$

according to the study by Groot and Warren, and  $r_c$  is the cutoff radius ( $r_c = 1.0$ ). The dissipative force is a friction force that acts on the relative velocities of beads, defined by

$$\mathbf{F}_{ij}^D = -\gamma \omega^D(r_{ij}) (\hat{\mathbf{r}}_{ij} \cdot \mathbf{v}_{ij}) \hat{\mathbf{r}}_{ij} \quad (4)$$

and the random force, compensating the loss of kinetic energy due to the dissipative force, is defined by

$$\mathbf{F}_{ij}^R = \sigma \omega^R(r_{ij}) \theta_{ij} \hat{\mathbf{r}}_{ij} \quad (5)$$

where  $\mathbf{v}_{ij} = \mathbf{v}_i - \mathbf{v}_j$ ,  $\gamma$  is the friction coefficient,  $\sigma$  is the noise amplitude,  $\omega^D(r_{ij})$  and  $\omega^R(r_{ij})$  are weight functions vanishing for  $r > r_c$  that describe the range of the dissipative and random forces, and  $\theta_{ij}$  is a randomly fluctuating variable with Gaussian statistics:

$$\langle \theta_{ij}(t) \rangle = 0, \quad \langle \theta_{ij}(t) \theta_{kl}(t') \rangle = (\delta_{ik} \delta_{jl} + \delta_{il} \delta_{jk}) \delta(t - t'). \quad (6)$$

In order to satisfy the fluctuation-dissipation theorem and for the system to evolve to an equilibrium state that corresponds to the Gibbs canonical ensemble, only one of  $\omega^D(r_{ij})$  and  $\omega^R(r_{ij})$  can be chosen arbitrarily and the other one is then fixed by the relation<sup>4,5</sup>

$$\omega^D(r_{ij}) = \left[ \omega^R(r_{ij}) \right]^2 = \omega(r_{ij}) \quad (7)$$

And the values of parameters  $\gamma$  and  $\sigma$  are coupled by

$$\sigma^2 = 2\gamma k_B T \quad (8)$$

where  $T$  is the absolute temperature, and  $k_B$  is the Boltzmann constant.

In the DPD method, reduced units are adopted for all physical quantities.<sup>5</sup> The units of mass, length, time, and energy are defined by  $m$ ,  $r_c$ ,  $\tau$ , and  $k_B T$ , respectively. The time unit  $\tau$  can be formulated by

$$\tau = \sqrt{(mr_c^2) / k_B T} \quad (9)$$

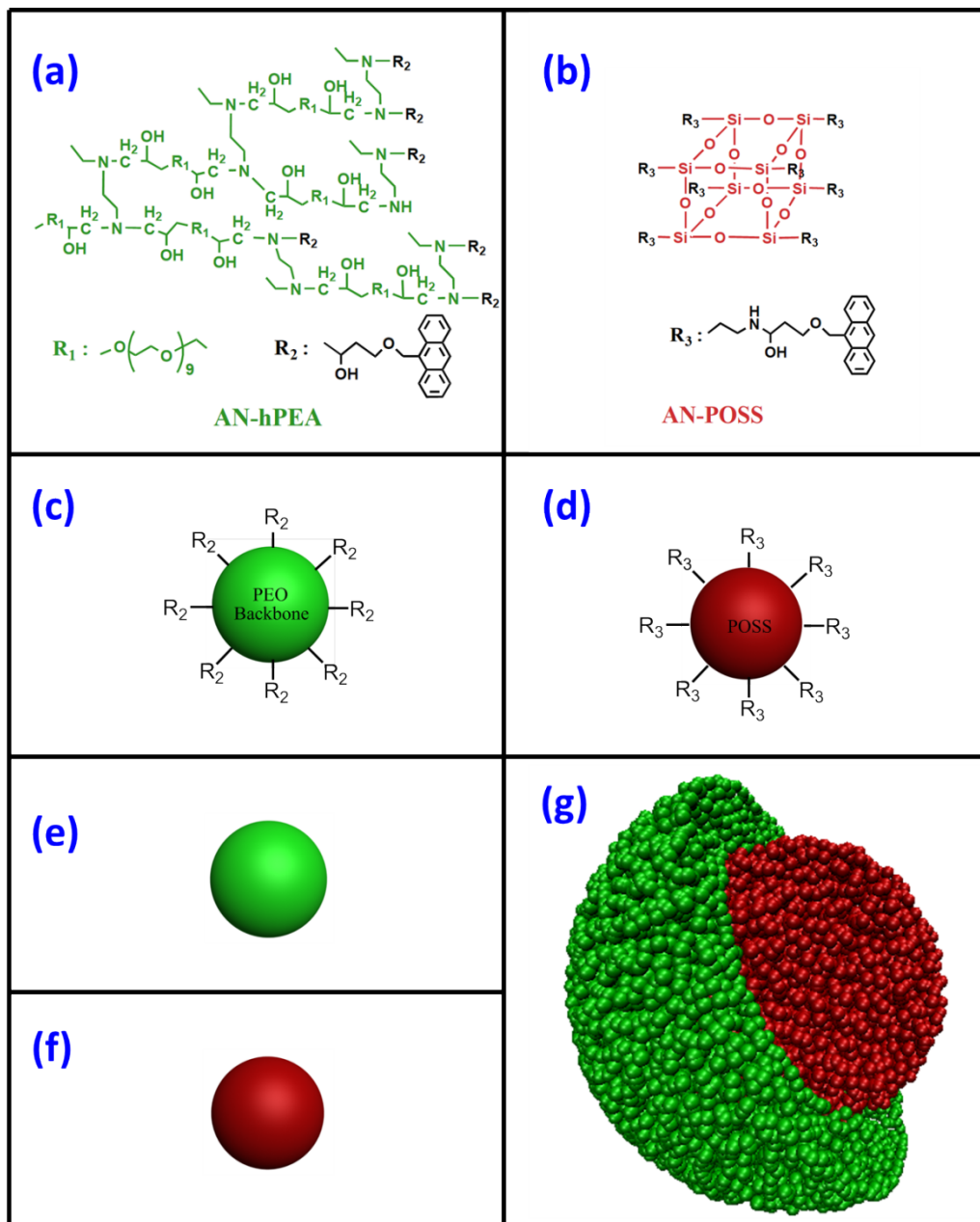
and the real value can be estimated by matching the simulated lateral diffusion coefficient to the experimental measured value.

### Model and Condition

Hyperbranched polymers have received widespread interest because of their easy synthesis, unique structures, and properties. Scheme S1a shows the chemical structure of anthracene ended hyper branched poly(ether amine) (AN-hPEA). The hyperbranched polymer consists of poly (ether amine) (PEA) backbone and anthracene terminal groups. Inspired by the sphere model of dendrimer, we constructed a coarse-grained model of AN-hPEA as is typically shown in Scheme S1c.

Scheme S1b shows the molecular structure of anthracene-ended polyhedral oligomeric silsesquioxane (AN-POSS). AN-POSS is comprised of POSS and

anthracene, where POSS locates in the center and anthracene acts as peripheral group. Since POSS is often regarded as the smallest silica nanoparticle, a sphere model of AN-POSS was constructed in Scheme S1d. Note that  $R_2$  and  $R_3$  are both anthracene groups, therefore, the models of AN-hPEA and AN-POSS are further simplified into single spheres (Scheme S1e, f).



**Scheme S1** (a) and (b) molecular structure of AN-hPEA and AN-POSS; (c) and (d) coarse-grained model of AN-hPEA and AN-POSS; (e) and (f) simplified model of AN-hPEA and AN-POSS; (g) cross-section of the incipient model of CSM.

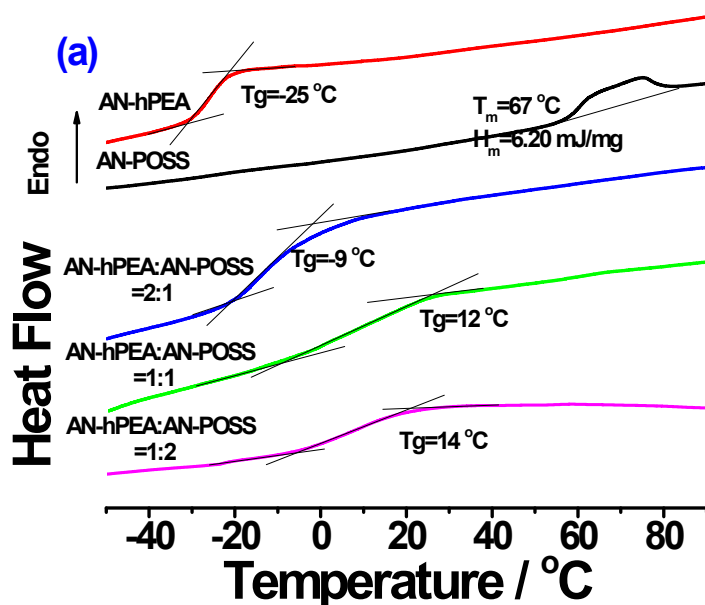
The main interaction between AN-POSS and AN-hPEA is the  $\pi$ - $\pi$  interaction of anthracene which is similar to the interaction between AN-POSS and AN-POSS or between AN-hPEA and AN-hPEA. Based on the DSC results, thus, an assumption is made that the interaction (F) between A and B satisfies  $F_{AB} = F_{BA} = F_{AA} = F_{BB}$ . Moreover, amphiphilic AN-hPEA is not soluble in hot water as the hydrogen bond between hPEA and water breaks under high temperature. In other words, the whole process is restricted in a single microsphere.

The incipient model generated is shown in Scheme S1g. The red beads AN-POSS were initially located in the sphere with radius  $r_A = 7r_c$ , while the green beads AN-hPEA were in the concentric spherical shell with thickness  $r_A = 4r_c$ . All the simulations were carried on a limited sphere space ( $22 \times 22 \times 22$ ) with periodic boundary conditions employed. The NVT ensemble was adopted, where  $T = 1.0$  corresponds to the temperature of  $85^\circ\text{C}$  in reality. A smaller value of time step ( $\Delta t = 0.0002\tau$ ) was chosen to ensure steady diffusion process. The friction coefficient  $\gamma$ , noise amplitude  $\sigma$ , and number density  $\rho$  were set to 4.5, 3.0, and 3.0, respectively. The interaction between identical species was set to be 25, while the interaction parameters between different species were all fixed as 100, implying that different species are incompatible. To capture all the equilibrated structures,  $3.0 \times 10^6$  DPD steps were carried out for the system.

### 3. Results

#### 3.1 DSC thermograms of AN-hPEA, AN-POSS and their corresponding composites

Figure S1a shows DSC thermograms of AN-POSS/AN-hPEA composites characterized by DSC as well as pure AN-hPEA and AN-POSS as references. hPEA-AN takes a glass transition at temperature around  $-26.3\text{ }^{\circ}\text{C}$  ( $T_g$ ), which should be ascribed to the presence of PEO chains in the backbone of hPEA-AN. The temperature for melting point of the crystallized POSS-AN is about  $62\text{--}75\text{ }^{\circ}\text{C}$ . The composites of hPEA-AN/POSS-AN with different formulation exhibit only one glass transition ( $T_g$ ), which increases with the increasing content of AN-POSS. These DSC results indicate that AN-hPEA and AN-POSS can mix homogeneously in varies ratios. Furthermore, according to Figure S1b, no phase separation was found for AN-POSS/AN-hPEA composite after several heat-cool cycles. In other words, the homogeneous structure is the stable state while the core-shell structure is meta-stable state. Thus the transition from core-shell structure to homogeneous structure is thermodynamically feasible.



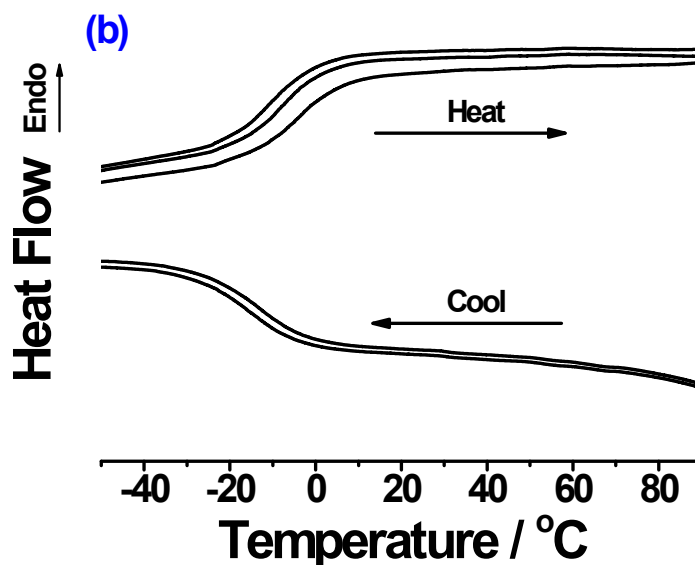


**Figure S1.** (a) DSC thermograms of AN-hPEA, AN-POSS, and their corresponding AN-hPEA/AN-POSS composites (weight ratio: 2/1, 1/1 and 1/2). (b) DSC Heat-Cool thermograms of AN-hPEA/AN-POSS=2/1 composite. The scans were run at a heating rate of 10 °C/min.

### 3.2 TEM images of Cross-section, SEM images and DLS of CSM along thermal annealing at 85 °C for different times

As shown in Figure S2, SEM images reveal that CSM keeps uniform-size along annealing. No fusion or diffusion was observed, indicating that the diffusion of AN-POSS only takes place in a confined space. The material exchange between CSMs is forbidden as water is not a good solvent for either AN-hPEA or AN-POSS. It is also supported by the low PDI data of DLS.

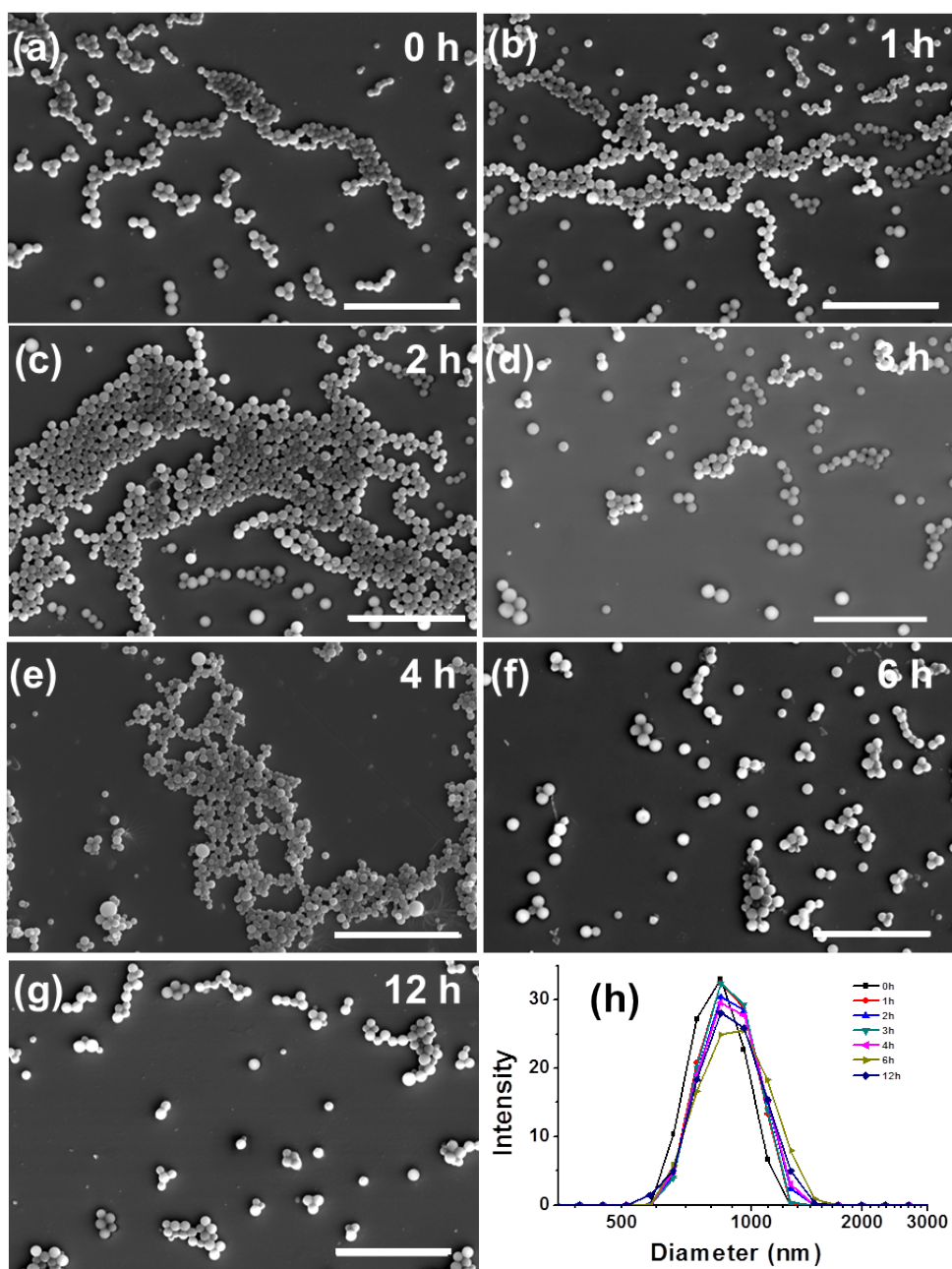


**Figure S2** SEM images and DLS data of CSM annealed at 85 °C. Scale bar 10  $\mu$ m.

As shown in Figure S3, the thickness of shell decreased along annealing and the shell almost disappeared after 6 hours of annealing. The boundary between core and transition layer cannot be observed neither.

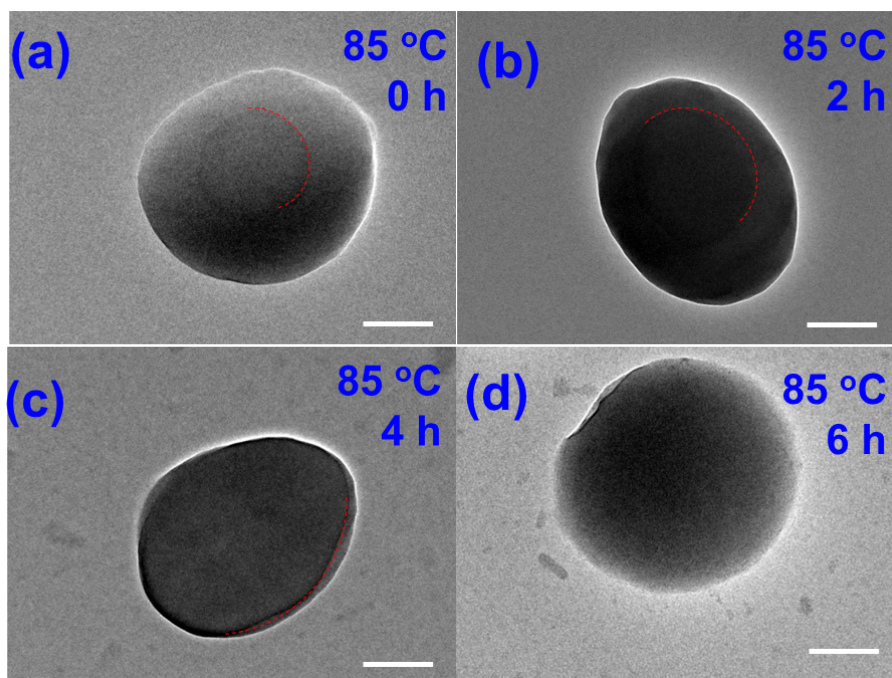


**Figure S3** TEM images of cross-sections of CSM upon different annealing time (85 °C). Scale bar 200nm.

### 3.3 Corresponding spatial distribution of AN-POSS in CSM along the radius direction at different annealing timesteps according to DPD simulation.

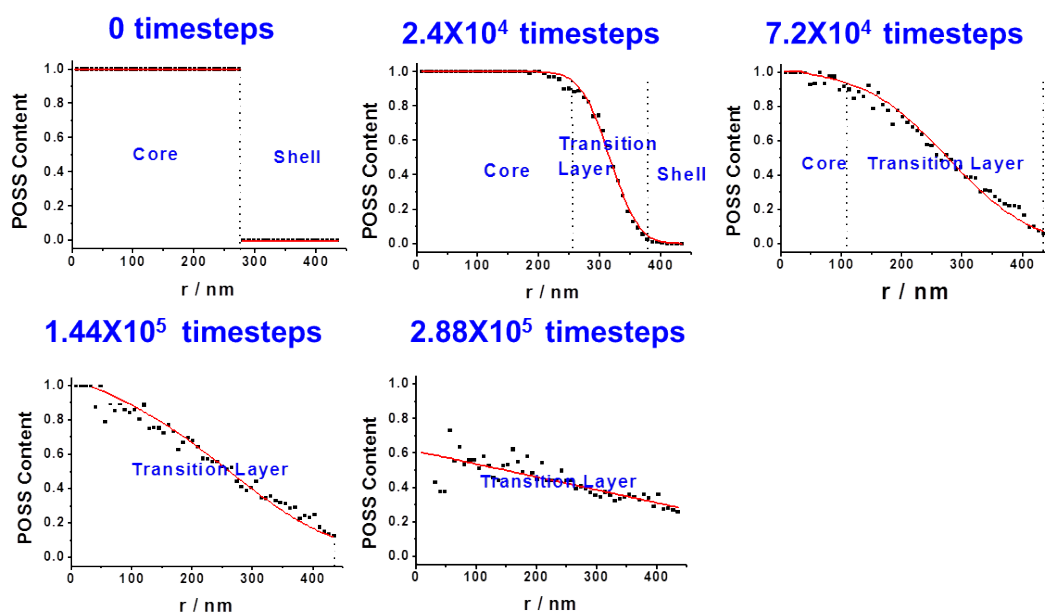


**Figure S4** Corresponding spatial distribution of AN-POSS in CSM along the radius direction at different annealing timesteps according to DPD simulation. Note:  $1.2 \times 10^5$  timesteps corresponding to 1 hour of thermal annealing.

### 3.4 Fick's second law of diffusion to stimulate the diffusion of AN-POSS in CSM

Fick's second law of diffusion<sup>8-10</sup> (Equation 10) is used to stimulate the migration of AN-POSS from the core to shell of CSM.

$$\frac{\partial C}{\partial t} = D \frac{\partial^2 C}{\partial r^2} \quad (10)$$

Where  $D$ ,  $C$ ,  $t$  and  $r$  are the diffusion constant, concentration, time and radial axis, respectively. Equation (10) can be expressed as follows<sup>10</sup>:

$$C_{(r)} = \frac{C_0}{2} \left\{ \operatorname{erf} \left[ \frac{(r_0 - r)}{2\sqrt{D \cdot t}} \right] + \operatorname{erf} \left[ \frac{(r_0 + r)}{2\sqrt{D \cdot t}} \right] \right\} - \frac{\sqrt{\frac{D \cdot t}{\pi}} \cdot \left\{ \exp \left[ \frac{-(r_0 - r)^2}{4 \cdot D \cdot t} \right] - \exp \left[ \frac{-(r_0 + r)^2}{4 \cdot D \cdot t} \right] \right\}}{r} \quad (11)$$

Equation (11) gives the concentration of AN-POSS along the radial axis at different times of thermal annealing.  $C_0$  is the concentration in the core of crystallized AN-POSS aggregation and can be regarded as 1.0 (100%).  $R_0$  is the radius of interface of core and shell, 275 nm. Based on the shell thickness of CSM at the different time of thermal annealing determined by TEM, the diffusion constant ( $D$ ) of AN-POSS in the shell of AN-hPEA at different temperatures can be calculated according to Equation (11). The POSS content at the boundary of AN-POSS and AN-hPEA obtained by TEM was regarded as 0.95. Take CSM annealed at 85 °C for 4 h as an example:  $t = 14400$  s,  $r_0 = 275$  nm, the thickness of shell is 65 nm thus  $r = 435 - 65 = 370$  nm,  $C_{(370)} = 0.95$ . Thus  $D$  is the only unknown parameter and can be dissolved by Mathcad. The diffusion constant ( $D$ ) is an average of several annealing time (85 °C:  $t = 2$ h, 4h, 6h; 75 °C = 6 h, 12h; 85 °C = 24 h, 48h).

The diffusion constant ( $D$ ) calculated according to equation (11) was shown in Figure S4. The diffusion constant ( $D$ ) of AN-POSS at 85, 75, and 65 °C is 0.120, 0.038, and 0.009 nm<sup>2</sup>/S, respectively. The diffusion constant is very low, and increases almost 13 times when the temperature increased from 65 to 85 °C. The low diffusion constant might be ascribed to that AN-POSS as nanoparticles is much bigger than the low-molecular weight molecules, resulting in the less mobility and slower diffusion in the polymer matrix. According to the linear Arrhenius plot (Figure S4),

the diffusion activation energy ( $Q$ ) is calculated to be 130.4 kJ/mol. The high diffusion activation energy might be also ascribed to the nature of AN-POSS as nanoparticles.

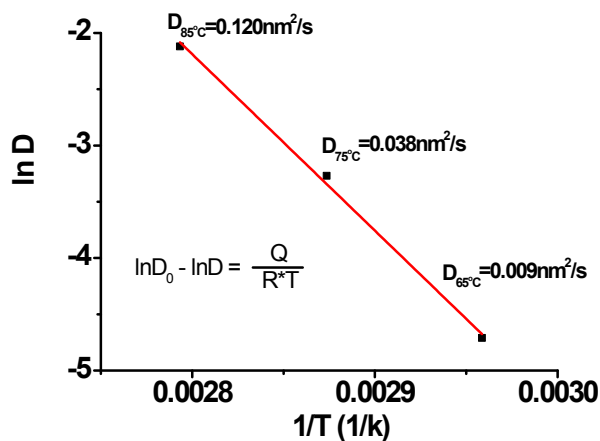


**Figure S5.** Arrhenius fitting of the diffusion constant ( $D$ ) of AN-POSS in AN-hPEA annealing at 85, 75 and 65 °C

### 3.5 Photo-cross-linking of CSM through the photo-dimerization of AN

**Photo cross-linking of CSM:** The solution of assemblies was stirred 2 hours under  $N_2$  atmosphere to remove oxygen in bottle. Then it was exposed to a 365 nm ultraviolet LED lamp (Uvata, China) whose intensity is 8.4 mW/cm<sup>2</sup> to lead to the photo-dimerization of anthracene moieties. The UV-vis tracing of crosslinking process (Figure S5a,b) were carried out with a UV-2550 spectrophotometer (Shimadzu, Japan). Taking the samples annealed for 3h as an example, the dimerization degree of AN groups is around 75 % after exposure of 365 nm UV-light for 15 min, and remains in further irradiation. Thus the irradiation time was set as 15 min.

**Solvent resistance of cross-linked CSM:** Cross-linked CSM (pre-annealed for 3h) was dissolved in THF to study the stability of cross-linked CSM in extreme conditions. Its TEM image is shown in Figure S5c. The shell expands several times while the core keeps well. This can be explained by the fact that the cross-linked hPEA shell swelling in THF.

**Heat resistance of crosslinked CSM:** The crosslinked CSM (pre-annealed for

3h) was heated at 85 °C for further 6 h (Figure S5d) and 12h (Figure S5e). The morphology keeps well, indicating that crosslinked CSM can resist further heat treatment. This should be ascribed to the cross-linked structure limited the diffusion of AN-POSS.

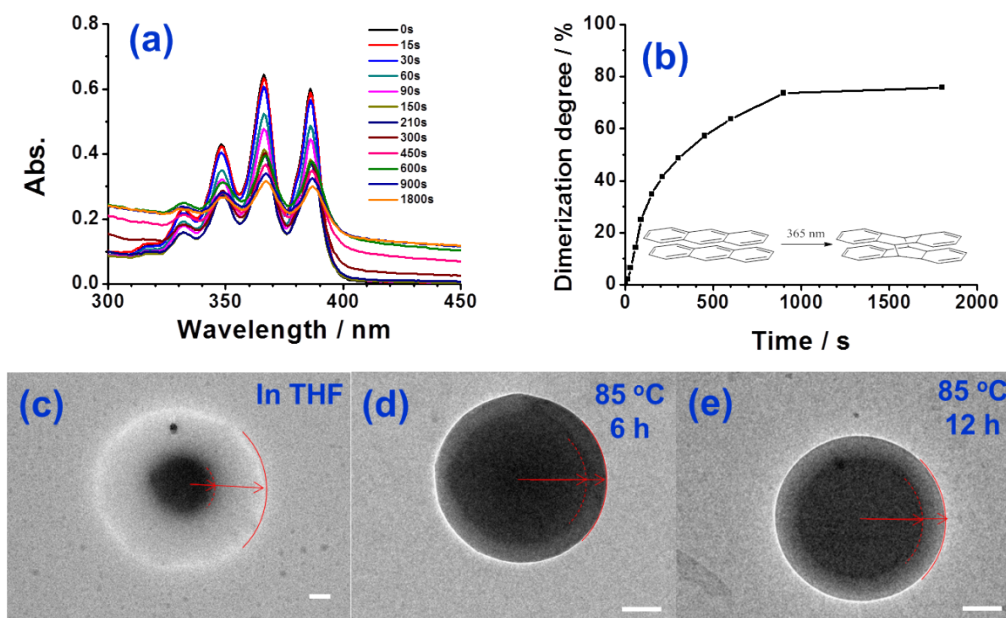


**Figure S6** (a) kinetics of UV crosslinking of CSM; (b) plots of crosslinking density of different time. (c) TEM image of crosslinked CSM dissolved in THF. (d) and (e) TEM images of cross-linked CSM after further annealing at 85 °C for 6 and 12 hours, respectively. The CSM studied here are all pre-annealed at 85 °C for 3 hours. Scale bar 200 nm.

### 3.6 Young's modulus of CSM determined by AFM

AFM is powerful to detect the mechanical properties of materials with nano-scale, and provide some insights into the fine details of polymer surfaces and interfaces.

The Young's moduli of AN-POSS/AN-hPEA composites are also studied by AFM for reference. (Figure S6) The AN-POSS/AN-hPEA composites are prepared by dropping casting of dioxane solution of AN-hPEA and AN-POSS mixture and dried by vacuum for 48 h.

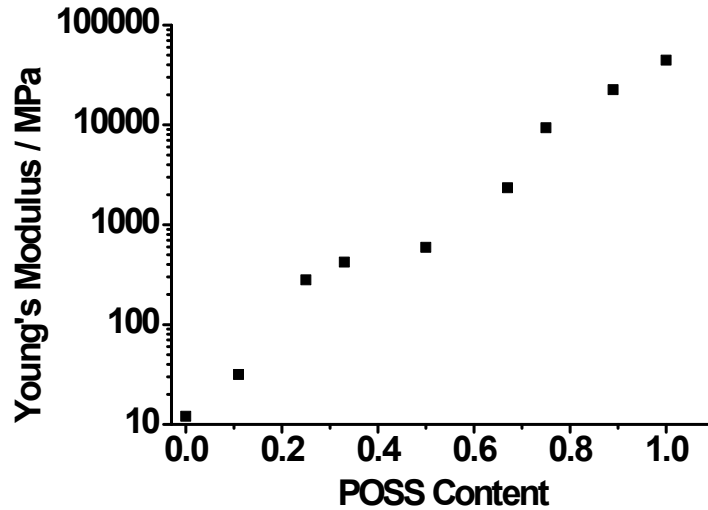


**Figure S7.** The Young's modulus of AN-POSS/AN-hPEA composites with different POSS content.

#### 4 References:

1. Z. Su, B. Yu, X. Jiang and J. Yin, *Macromolecules*, 2013, 46, 3519-3528.
2. P. J. Hoogerbrugge and J. M. V. A. Koelman, *Europhy. Lett.*, 1992, 19, 155.
3. J. M. V. A. Koelman and P. J. Hoogerbrugge, *Europhy. Lett.*, 1993, 21, 363.
4. P. Español and P. Warren, *Europhy. Lett.*, 1995, 30, 191.
5. R. D. Groot and P. B. Warren, *J. Chem. Phys.*, 1997, 107, 4423-4435.
6. Y.-J. Sheng, C.-H. Nung and H.-K. Tsao, *J. Phys. Chem. B*, 2006, 110, 21643-21650.
7. Y. Xu, J. Feng, H. Liu and Y. Hu, *Mol. Simul.*, 2008, 34, 559-565.
8. J. Crank, *The Mathematics of Diffusion*, Oxford University Press, 1979.
9. S.-J. Yook and K.-H. Ahn, *Appl. Phys. Lett.*, 2009, 94, 191909-191912.
10. F. D. Fischer and J. Svoboda, *Prog. Mater. Sci.*, 2014, 60, 338-367.